Received: 20 November 2023 | Revised: 21 February 2024 | Accepted: 2 March 2024

DOI: 10.1002/rra.4268

RESEARCH ARTICLE

WILEY

Temporal variation of braided intensity and morphodynamic changes in a regulated braided river using 2D modeling and satellite images

Behnam Balouchi[1] | Nils Rüther[2] | Kordula Schwarzwälder[1]

[1]Department of Civil and Environmental Engineering, Norwegian University of Science and Technology, Trondheim, Norway

[2]Chair of Hydraulic Engineering, Technical University of Munich, Munich, Germany

Correspondence
Behnam Balouchi, Department of Civil and Environmental Engineering, Norwegian University of Science and Technology, Trondheim, Norway.
Email: behnam.balouchi@ntnu.no

Funding information
Nederlandse Organisatie voor Wetenschappelijk Onderzoek; Svenska Forskningsrådet Formas; Bundesministerium für Bildung und Forschung; Norges Forskningsråd; Österreichische Forschungsförderungsgesellschaft; European Union, Grant/Award Number: 776608

Abstract

The river morphology of a braided-type river is rather complex. High sediment transport rates and frequently changing discharges are the cause of dynamic planform evolution. Over the past few decades, scientific attention has been directed toward understanding the coexistence of alternating bars and the consequent emergence of confluences and divergences, all of which interact intricately with the process of bank erosion. It is still rather challenging to estimate or predict the total sediment transport rate in this type of river, especially by considering various hydrologic data and climate effects. This study is focused on the reach of the Devoll River in Albania, located upstream of the Banja dam. Understanding the morphodynamics of this river reach holds significance due to the expanding delta upstream of the dam reservoir. The objectives of the two-dimensional depth-averaged approach of the present study are to investigate the temporal variation of braided intensity of Devoll River and the effect of using a discharge hydrograph from hydrologic data compared to the regulated one from the upstream dam on the morphodynamics and sediment transport of the river. After evaluating various parameters such as 11 different sediment transport functions, the best results were reached for a cell size of 5×5 m^2, Manning roughness coefficient of 0.03, Meyer-Peter and Müller's sediment function, Hayashi et al. (1980) hiding function, and Van Rijn bed roughness predictor in this study. In addition, the results of comparing satellite images and modeling the river from 2019 to 2023 show that the braided index decreased, and this can be due to the fact that the real scenario of the river has a regulated discharge compared to the non-regulated discharge from hydrologic data, in the mentioned period.

KEYWORDS
2D modeling, braided intensity (BI), braided river, morphodynamics, regulated discharge, satellite images

1 | INTRODUCTION

A braided river is a fascinating and intricate natural phenomenon that captures the imagination with its complex network of channels and shifting patterns. Characterized by multiple interwoven channels that split, rejoin, and merge, braided rivers showcase the dynamic nature of water flow. These rivers are typically found in regions with high sediment supply, steep gradients, and frequently changing discharges (Ashmore, 1982; Balouchi et al., 2022; Olsen, 2021; Yassine et al., 2023). These factors contribute to the continuous alteration of the channel's shape and the evolution of the river over time. In addition to human activities and natural disasters such as earthquakes and landslides, the morphology of this type of river is changing frequently with seasonal varying hydrology, dominated by a rather dry, long summer and winter month with intense but rather short rainfall events (Ashworth et al., 1994; Balouchi et al., 2023; Williams, Brasington, et al., 2016).

There are three approaches for assessing the morphodynamics of braided rivers. The first and second approaches comprise experimental and field studies, respectively. Numerous experimental and field studies have been conducted to investigate the morphological changes in braided rivers. Examples of such studies can be found in the literature, including Ashmore (1982), Ashworth et al. (1994), Bertoldi et al. (2010), Egozi and Ashmore (2009), Kasprak et al. (2015), and Schuurman et al. (2013). The third approach involves 1D, 2D, and 3D numerical modeling which is the focus of this study. The numerical modeling of morphodynamics in braided rivers has emerged as a valuable tool for understanding the complex processes shaping these above-mentioned dynamic river systems. In recent years, numerous studies have utilized numerical models to simulate and analyze the hydrodynamics, sediment transport, and morphological evolution of braided rivers. Among them, Sun et al. (2015) presented a physics-based morphological model for simulating the evolution of braided channels, incorporating a hydrodynamic sub-model for rapidly varying flows and a sediment transport sub-model for non-uniform sediments. Their model generally predicted channel patterns and morphological changes observed in a flume experiment well, shedding light on the mechanisms behind the evolution of multi-thread flows through grain sorting and fluid-sand interaction.

Modeling braided rivers with a 2D depth-averaged morphodynamic model named Delft3D (Deltares, 2011) is also interesting for researchers in the last two decades. Williams, Measures, et al. (2016) evaluated the performance of a physics-based numerical model (Delft3D) in predicting the morphodynamics of a braided reach during a high-flow event. The model calibration and sensitivity analysis demonstrate the effectiveness of using natural experiment data sets for model testing and provide insights for applying the Delft3D model to other rivers. Lotsari et al. (2018) also used Delft3D to model a braided river with moderate and small floods. Their results confirmed that erosion and deposition were in total greater during the receding phase than during the rising phase of the discharge hydrographs. Moreover, Shampa (2019) also used this model to study the interaction between the braided bar and adjacent channel during a flood. Their 2D model could reproduce the major physical processes that are responsible for the growth of the bar in a braided river.

Antoniazza et al. (2019) used a 1D and 2D model named Basement (Faeh et al., 2011) to simulate an Alpine braided river of a laboratory experiment to evaluate the bed-material transport. Their results showed that the 1D modeling leads to substantial local errors in transport rate estimates and 2D modeling showed that a large proportion of the total transport was concentrated into one main channel during the low flow event. Kasprak et al. (2019) developed a framework that combines steady-state, 2D CFD hydraulics with a rule-based sediment transport algorithm to predict sediment particle mobility and river evolution and transport paths in a braided river. They used both MoRPHED open-source code (Hafen & Kasprak, 2019), and Delft3d in their study. Their hypothesis was that morphodynamic simulation can be approximated using a steady flow set of the peak discharge, instead of the whole hydrograph and reduced the time cost of the model or increased the spatial resolution of the model. Their results showed over and under-predicted in some points and good agreement in some other points with the measured data.

Dubey et al. (2020) used satellite altimetry and 1D flow modeling by HEC-RAS to retrieve the river roughness as an important property of a braided river. Yang (2020) modeled braiding evolution processes and avulsion activities in a gravel-bed river and compared their results with the measured data in the laboratory. They found that the highest probability for a channel bend to generate an avulsion is with a curvature radius of around 2.0–3.3 times the average anabranch width. Prasujya and Nayan (2021) used braided indices to quantify the morphodynamics of a braided river. In a study carried out by You et al. (2022), the authors examined the impact of natural flow regimes, dams, and human activities like farming, urbanization, and mining on the morphological changes of four braided channels in China. The findings indicated that the two dams had a minimal effect on the channel morphology, and the morphological changes in most reaches were similar. Yassine et al. (2023) utilized a 2D hydro-morphological modeling approach called TELEMAC2D (Hervouet & Ata, 2017) to simulate the transformation of a river reach from a single-channel section to a braided river reach following specific flood events. Their findings highlight the difficulty in accurately reproducing complex morphology, attributing this challenge to factors not accounted for in the model, such as the entire grain-size distribution or suspended load. They suggest that the uncertainty and randomness of channel evolution, particularly during flood events, contribute to the models' inability to accurately predict river branching.

In addition to the literature review discussed in the earlier part, there are several other review papers available in the existing literature about modeling braided rivers. For instance, Williams, Brasington, et al. (2016) published a review paper specifically focused on the taxonomy of morphodynamic modeling of braided rivers. They emphasized the importance of addressing three key challenges to advance the field of morphodynamic modeling for braided rivers: (i) accurately representing flow and sediment transport, (ii) effectively addressing temporal and spatial scaling, and (iii) improving model calibration, sensitivity, uncertainty analysis, and validation techniques.

The present study aims to contribute to existing literature by addressing these three challenges as well. In more detail, the novel contribution of the present study is using a 2D numerical modeling approach to simulate the morphodynamics of a complex braided river by focusing on:

a. Sensitive analysis of various effective parameters such as three cell size, five roughness coefficients, 11 transport functions, five hiding functions, three-bed roughness predictors, and so forth on the morphodynamics of a braided river.
b. Evaluating the variation of the Braided Index (BI) of chosen reach over time.
c. Investigate the effect of using a non-regulated discharge hydrograph from natural hydrologic data and a regulated one from an upstream hydropower dam on the morphodynamics of the river.

2 | MATERIALS AND METHODS

2.1 | Study area

The Devoll River is located in southeast Albania and has various topographical features. One of them can be found downstream of the location Kokel, where the terrain changes from a v-shaped valley to an open, more flat type of valley. Here, the Devoll River forms a complex system of multiple branches forming a braided river. The Banja catchment and study area of this study are shown in Figure 1. In 2016 and 2020, two large hydropower dams were impounded and started to produce electricity on the Devoll River. The Banja Hydropower plant is downstream of the Kokel station and the Moglice power plant is upstream of the Kokel station.

The Banja reservoir was impounded in 2016 and has a storage capacity of approximately 400 million m^3. The mean annual production amounts to around 255 GWh. The catchment area of the reservoir has a size of 2900 km^2 and is located within a mountainous region with a diversified topography. Moglice Dam is the second hydropower plant on the Devoll River that was impounded, and commercial operations started in 2020. The reservoir has a storage capacity of approximately 380 million m^3 and a surface area of approximately 7.2 km^2. The average annual production is approximately 450 GWh.

The Devoll catchment, situated in Mediterranean Europe, is recognized as a hotspot for erosion, experiencing significant soil loss due to the combined impact of high precipitation erosivity and steep topography (Mouris et al., 2022). Due to this significant sediment input from the catchment, the Banja reservoir is of particular interest from a hydromorphological perspective, as it serves as a large sink for sediments.

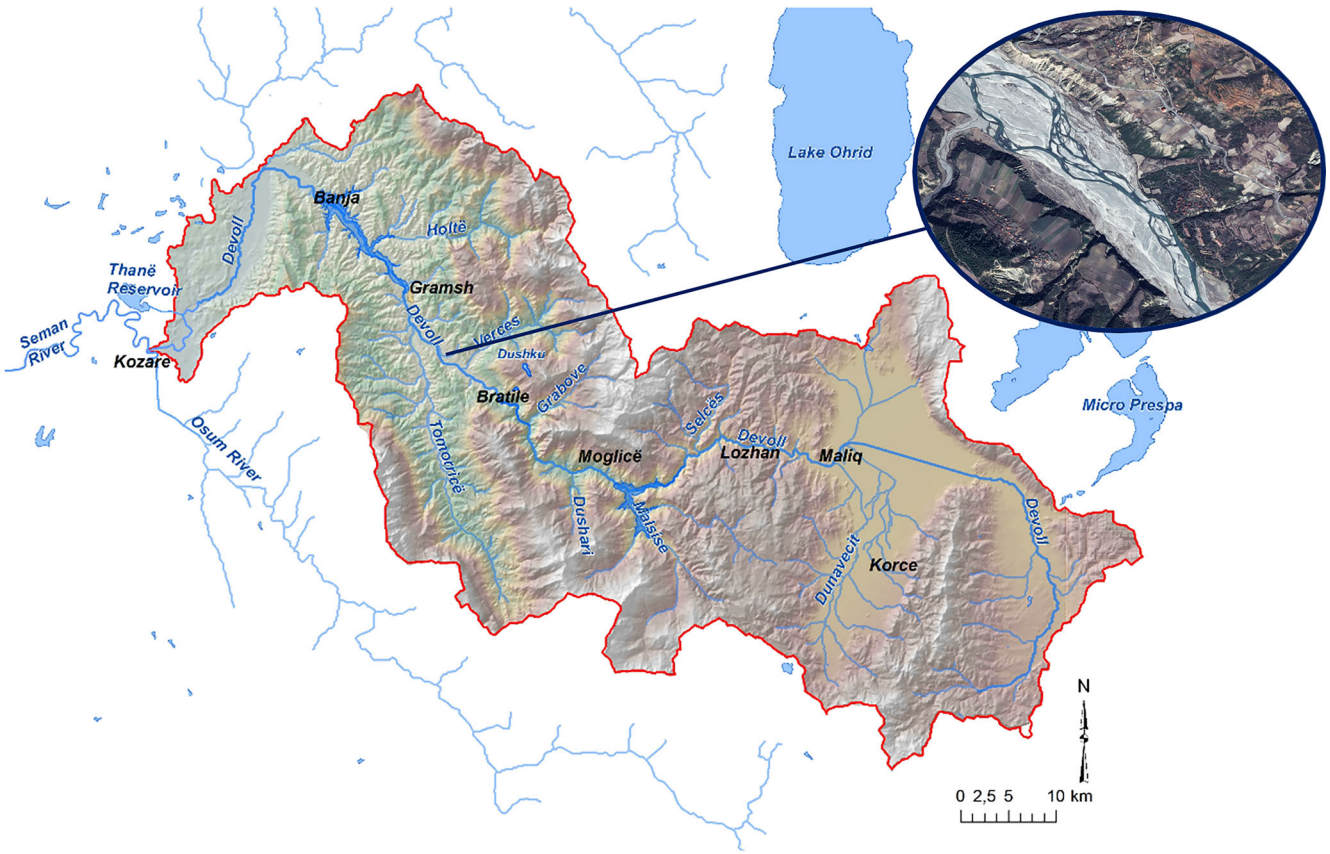

FIGURE 1 The Banja catchment and the Devoll River (adopted from Norconsult, 2011). [Color figure can be viewed at wileyonlinelibrary.com]

2.2 | Data availability

2.2.1 | Measured data

In the current study, the topography data used in modeling are a digital terrain model (DTM). This DTM was prepared from the ground classified points of the Lidar data taken on 9 February 2019. In addition, hourly measurements of discharge have been available at the Kokel gauging station for some years. This is obtained using the acoustic backscatter signal from two side-looking H-ADCPs (Horizontal acoustic Doppler Current Profiler; 0.6 and 1.2 MHz). Nevertheless, these measurements are only available for water depths at the gauging station exceeding 1 m (Pesci et al., 2023). In addition, using the pebble count method in the focused area of this study, the substrate grain size distribution curve was measured in the field, describing the bed material by D_{50} of 19 mm, the mean particle size of 25 mm, and the standard deviation of 1.49. Figure 2 shows the used sediment distribution curve in this study.

2.2.2 | Satellite images

The satellite images used in this study are from Sentinel-2 L2A. The resolution of these images is 10 m. The Normalized Difference Water Index (NDWI) version of these images was used. The NDWI is used to detect changes related to water bodies. As water bodies absorb light in the visible to the infrared electromagnetic spectrum, NDWI uses green and near-infrared bands to identify water bodies. These images are shown and discussed in the discussion of the results section.

2.3 | Numerical model

In the current study, the HEC-RAS 2D model is considered for the numerical morphodynamic simulation. HEC-RAS 2D (Hydrologic Engineering Centers' River Analysis System 2D) is a hydraulic modeling software widely used in the field of river and floodplain hydrodynamics. This numerical model is designed to simulate 2D water flow and sediment transport in natural or constructed channels, providing valuable insights into flood inundation, channel morphology, and hydraulic behavior. HEC-RAS 2D uses shallow water equations (SWE) as its fundamental governing equations. These equations are the 2D continuity equation, expressing the conservation of mass, and the 2D Saint-Venant equations, which account for momentum and energy conservation. By discretizing these governing equations, HEC-RAS 2D is able to solve the water surface elevations, flow velocities, and sediment problems. In this study, the SWE with an Eulerian–Lagrangian approach (SWE-ELM) are used to discretize the acceleration terms in the momentum equation (Hydrologic Engineering Center, 2021). This technique is advantageous for handling large-time steps while ensuring stability and it is recommended by the HEC-RAS team for sediment modeling. In addition, the boundary conditions used in this study are the discharge hydrograph for the upstream boundary condition (which is represented in the next sections) and normal depth with a slope of 0.009 for the downstream boundary condition.

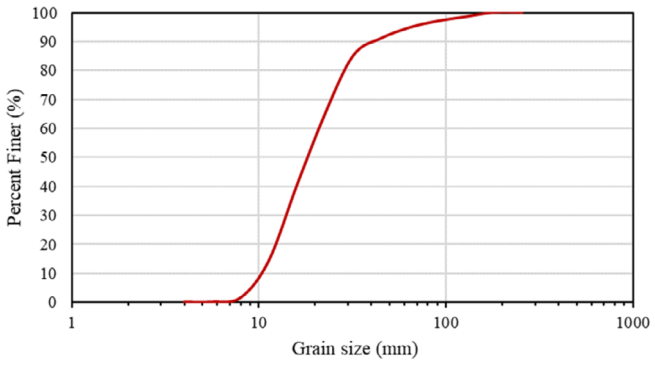

FIGURE 2 Grain size distribution curve. [Color figure can be viewed at wileyonlinelibrary.com]

2.3.1 | Sediment transport functions

Eleven different sediment transport functions named Ackers and White, Engelund and Hansen, Laursen-Copeland, Meyer-Peter and Müller (MPM), Toffaleti, MPM-Toffaleti, Yang, Wilcock and Crowe, Soulsby-Van Rijn, Van Rijn, and Wu et al. are evaluated in this study. Since the equations and details of these methods can be found in the literature, a brief overview of each is provided as follows.

Ackers and White

The original Ackers and White model, developed in 1973, aimed to estimate the total load of uniform material based on laboratory data (Ackers & White, 1973). They derived this equation through dimensional analysis, without accounting for grain shear partition. Later, Day (1980) and Proffitt and Sutherland (1983) enhanced the original method by introducing a hiding and exposure correction factor. This adjustment made the method more accurate for non-uniform sediments. However, these adaptations did not fare well when applied to real-world field data. One of the main causes of this discrepancy is the uncertainty surrounding the source material distribution and the possibility of overpassing giving rise to a transported material distribution quite different in shape to the bed-material distribution. Wu (2007) delved into the Ackers-White formula's performance for graded sediments and highlighted its tendency to notably overestimate transport for fine sediments under 0.2 mm.

Engelund and Hansen

Engelund and Hansen (1967) represents a method for calculating the total load transport, originating from flume experiments and primarily focused on relatively consistent sand sizes. The Engelund and Hansen equation is the simplest formula for predicting sediment transport, directly dependent on stream power ($V^2\tau^{3/2}$) and the median grain size (d_{50}) of the material. Since it does not function as an "excess" stream power equation, it does not control for competence and often ends

up estimating lower sediment transports for large grain classes. Typically, Engelund–Hansen is more suitable for analyzing sandy systems.

Laursen–Copeland

Laursen (1958) introduced a sediment transport formula for total load, initially derived from flume experiments and later extended using data from the field. Later, Copeland and Thomas (1989) generalized the equation for gravel transport. A noteworthy feature of the Laursen–Copeland formula is its applicability across a wide range, spanning from silts to gravel sizes.

Meyer-Peter and Müller

The Meyer-Peter and Müller (1948) equation, derived from flume experiments with sand and gravel under flatbed conditions, serves as a bed-load formula. It was originally developed for uniform sediment beds. This study uses the version of MPM from Vanoni (1975). This version integrates a correction for form drag based on the roughness element ratio obtained from the Darcy–Weisbach bed friction factor. This correction isolates grain shear and computes sediment transport based on the bed shear component acting only on the particles. The MPM formula is best suited for uniform gravel beds and often predicts lower sediment transport values for finer materials like sands and silts.

Toffaleti

Toffaleti (1968) presents a total load function primarily designed for sand-sized particles. It follows the basic principles of the Einstein approach but introduces some refinements by replacing some of the empirical assumptions. The method is not based on excess shear but rather regression equations that take into account sediment and water properties, as well as hydraulic variables. Toffaleti's methodology divides the water column into four vertical zones and calculates the concentration for each zone using a simplified version of a Rouse concentration profile. These four zones are determined by theoretical inflection points and transitions in the vertical velocity profile.

MPM-Toffaleti

The Toffaleti bed-load transport method does not perform very well for gravel size or coarse particles. Consequently, there is an alternative to substitute the bed-load transport aspect in the Toffaleti equation with an estimate obtained from the Meyer-Peter and Müller formula (Williams & Julien, 1989). This combined equation is known as the MPM-Toffaleti formula.

Yang

Yang (1973, 1979, 1984) introduces an equation for total load sediment transport, where sediment movement is determined through the evaluation of stream power. This stream power is derived from the multiplication of velocity and shear stress. This function was developed and validated over a variety of flume and field data. This equation includes two separate relations for sand and gravel transport. According to the existing literature, the Yang transport equations often lead to overestimating transport, particularly for very coarse sands.

Wilcock and Crowe

Wilcock and Crowe (2003) formulated a bedload equation specifically designed for rivers characterized by well-graded (poorly sorted) sediment, encompassing both sand and gravel. This method is classified as a "surface" transport approach, grounded in the concept that the movement depends on the material directly interacting with the flow. According to this concept, it is the bed surface that mainly influences bed mobility. The riverbeds were often armored with notably less sand content on the surface compared to the subsurface. Hence, it is crucial for users to adopt active layer algorithms and choose gradations that accurately represent the properties of the bed surface, as had been done in this study.

Van Rijn

Van Rijn (1984a, 1984b, 1984c) solved the equations of motion of an individual bed-load particle, thereby calculating the saltation characteristics and the particle velocity based on the flow conditions and particle diameter. These calculations were conducted under the plane bed conditions to determine bed load transport. Initially, these formulas were suggested for well-sorted sediment distribution. However, adaptations were made for situations involving nonuniform sediments. This was accomplished by substituting the median grain size with the diameter of the specific grain class and adjusting the critical depth-averaged current velocity through a correction factor that accounts for hiding and exposure effects. These equations underwent rigorous validation through extensive field and laboratory data collected by various researchers.

Soulsby-Van Rijn

The Soulsby-Van Rijn formula was developed by adjusting the Van Rijn (1993) sediment transport equations through calibration, which involved introducing a new coefficient into the equations (Soulsby, 1997).

Wu et al.

Wu et al. (2000) introduced a correction factor to address the hiding and exposure aspects of transporting nonuniform sediments. This correction factor is designed to be a function of the hidden and exposed probabilities. These probabilities are statistically connected to the size and gradation of bed materials. Grounded on this concept, the equations to compute the critical shear stress of incipient motion developed. Additionally, the fractional bed load and suspended load transport rates of nonuniform sediment have been established. These equations have been tested against a wide range of laboratory and field data.

2.3.2 | Hiding functions

In cases where the bed consists of various grain sizes, larger particles are more likely to be exposed to the flow, whereas smaller particles tend to have a higher probability of being hidden from the flow. The inclusion of the hiding and exposure effect in the sediment transport formula varies based on the specific form of the transport

equation. In this study, Ashida and Michiue (1971), Egiazaroff (1965), Hayashi et al. (1980), Parker et al. (1982), and Wu et al. (2000) hiding functions were evaluated. As the related details and equations can be found in the literature, the methods are briefly explained as follows. These functions can be categorized into two approaches, as also outlined by Schendel et al. (2015). The first approach generally relates the grain diameter of the considered fraction in a sediment mixture (d_j) to the arithmetic mean grain diameter of the sediment mixture (d_a) or often the median grain diameter (d_{50}). The second approach is based on the probabilities of hiding and exposure.

Ashida and Michiue (1971), Egiazaroff (1965), Hayashi et al. (1980), and Parker et al. (1982) are based on the first approach. Egiazaroff (1965) hypothesized that the entrainment of a sediment grain occurs when its velocity aligns with the settling velocity in posed water. Then, he proposed a hiding coefficient, to compensate for the critical shear stress in such conditions. Okazaki (2001) noted that the Egiazaroff assumption yielded satisfactory outcomes when applied to nonuniform mixtures. In subsequent developments, the Ashida and Michiue (1971) formula emerges as a refined version of the original Egiazaroff (1965) formulation. Ashida and Michiue (1971) observed that the Egiazaroff (1965) equation underestimated the mobility of small particles (dj <0.4d_a) although it worked well for larger particles. dj is the representative diameter of a considered fraction in the sediment distribution and d_a is the median diameter of the sediment mixture (Paixão & Kobiyama, 2020). So, they proposed a conditional function based on the relation between dj and d_a. Subsequently, the Hayashi et al. (1980) equation can be seen as a reevaluated adaptation of the Ashida and Michiue (1971). This revision involves adjustments in the conditional function, which draws inspiration from the original Egiazaroff (1965) formulation. Parker et al. (1982) used the same approach to relate the hiding function to a simple relation between d_j and d_{50}.

In the second approach, Wu et al. (2000) introduced a correction factor based on predicting the probabilities of hiding and exposure effects in the nonuniform sediment bed surface. This factor is considered a variable influenced by the hidden and exposed probabilities, which are stochastically related to the size and gradation of bed materials. The approach was validated through comparisons with laboratory data and measurements of riverbed loads.

2.3.3 | Bed roughness predictors

By default, the user-defined Manning's roughness coefficient used for hydrodynamics is applied to determine the overall bed roughness. The evaluation of Manning's roughness coefficient is explained in Section 3.2. In addition, to consider the effect of variation of bed roughness based on sediment dynamics, three bed roughness predictors named Limerinos, Brownlie, and Van Rijn are used in this study. Activation of this parameter results in the model adopting a dynamic bed roughness approach, enhancing the ability to account for both shape roughness and form roughness of the river. These three methods are explained briefly as follows.

Limerinos

Limerinos (1970) introduced an equation based on the D_{84} and hydraulic radius, with no consideration for bed form mechanics to predict the bed roughness. This equation is best suited for coarse systems with gravel and cobble, where grain roughness is the primary source of channel roughness. The equation works well for Froude numbers <1. However, it has limitations. It does not consider the full range of sediment sizes, only using a representative diameter. This makes it less suitable for beds with poorly sorted materials.

Brownlie

Brownlie (1983) calculated bed roughness using bed form mechanics, focusing on larger rivers. His aim was to capture the non-linear drop in roughness when bed form dominated transport shifts from lower to higher regimes. Brownlie determines the bed form regime using hydraulic parameters, median grain size, and gradational distribution. He then applies separate equations for low and high regime transport to account for these shifts.

Van Rijn

The Van Rijn (1984c) alluvial roughness height predictor computes the total roughness as the sum of the grain (which is related to D_{90}) and dune roughness (which is related to the dune height and length). This method was developed to estimate bed roughness in both dune and plane bed conditions.

2.3.4 | Assessment indices

In this study, due to the lack of measured data in 2019, which is the date of the used DTM file in the modeling, satellite images were used to calibrate the model. Although this method is not so accurate, as a braided river is unstable and has evolved over time, this method can be acceptable by representing the river's evolution. For this purpose, a satellite image of 16 February 2019 was used, and the water inundation area of the satellite image was compared to the computed by numerical modeling. To reach this goal, I_u, or index of unmatched area, was introduced as an objective function. The higher value of I_u has the less unmatched area and consequently has a more accurate result. Unmatched area (m^2) refers to the summation of areas where the water inundation from the satellite image (observed) is different or unmatched from the model simulation. Equation (1) shows this index, where A_o is the observed area, and A_m is the modeled area.

$$I_u = \frac{A_o - [(A_o \cup A_m) - (A_o \cap A_m)]}{A_o} \times 100. \quad (1)$$

To find A_o, the satellite image is converted to the NDWI image. Then, the wet area was extracted using a Support Vector Machine, which is a supervised classification method. Afterward, other terms were computed in the ArcGIS® PRO by comparing the observed and simulated images.

Furthermore, as previously stated, the braided river represents an intricate and unsteady river type, and its instability is assessed using

diverse indicators, including the BI. The BI is calculated as follows (Kuo et al., 2017):

$$\mathrm{BI} = \frac{(\Sigma m + \Sigma l)}{\Sigma m}, \quad (2)$$

where Σm is the sum of the mainstream length and Σl is the sum of all lateral stream lengths. The mainstream channel was chosen by observing the most unchanged and largest reach along the river direction which can transfer most of the flow of the river. Other lateral streams are those that are not part of mainstream and are located around bars, junctions, or confluences.

3 | DISCUSSION OF RESULTS

According to the mentioned objectives of this study, the temporal variation of the BI is first evaluated using satellite images in this section. Then a 2D depth-averaged morphodynamic model is used to assess potential hypotheses, such as the impact of the regulated discharge released from the upstream hydropower dam, on the variation of the river's BI and its morphodynamics. The sensitivity analyses of important parameters and the results of the total load transport rate and suspended load concentration were also discussed in this section.

3.1 | Temporal variation of the BI by satellite images

Figure 3 presents the Sentinel-2 L2A satellite images from 2016 to 2023 with the NDWI. Through visual analysis of these images, it is evident that the braided intensity of the river has generally decreased from 2016 to 2023. In addition, the river paths are not constant and tend to change over the years which is the tendency of a braided river.

By analyzing the images in Figure 3, the BI was calculated and represented in Figure 4. According to this figure, the values of BI for 2016 to 2023 are 2.71, 2.64, 4.02, 2.44, 2.16, 1.46, 1.45, and 1.24, respectively. Generally, these values show a descending trend from 2016 to 2023 (except 2018 which is explained later in this section) which is probably due to the regulated discharge. This reduction rate is 0.07 from 2016 to 2017 and 0.28 from 2019 to 2020, which are the years before the impoundment of the Moglice Dam and after the Banja Dam. On the other hand, after impounding the upstream dam and starting to regulate the river reach in this study, the reduction rate of BI in the Devoll River changed to 0.7 from 2020 to 2021. This rate is 10 times greater than the reduction rate in 2016–2017 and 2.5 times greater than the reduction rate in 2019–2020 which probably shows the effect of starting to regulate the river.

Figure 9 illustrates the released discharge from the Moglice Dam which generally has frequent intermittent variations between 1 and 70 m^3/s, approximately. Delving into more detail, the minimum and maximum released discharge during the day typically range around 1 and 40 m^3/s, respectively. Notably, there are occasional hours with discharge peaks reaching approximately 70 m^3/s, approximately. This regulated discharge hydrograph leads to a reduction in morphological changes and a decrease in flow diversity in the targeted section of the Devoll River. Consequently, highly alternating river stretches undergo transformation into a single channel cutting through the valley, as depicted in Figure 3h.

Apart from the change in the discharge hydrograph of the river or changing the river to the regulated discharge river, the evolution of the river can be significantly impacted by human activities and natural calamities such as landslides. Landslides are a common occurrence in the catchment area because of the steep, unstable slopes composed of highly weathered and weak rock. This instability is exacerbated by the clearance of vegetation and the region's susceptibility to intense rainfall, which typically ranges from 600 to 1900 mm (International Hydropower Association, 2022). It is highly likely that the primary cause of the increased BI in Figure 4 is the landslide that occurred in 2018. This landslide obstructed the main pathway and amplified the instability or braiding intensity of the river. Therefore, it is highly probable that changes in the river path and dynamics are observed within our focused domain. Figure 5 depicts this landslide in 2018.

3.2 | 2D morphodynamic modeling

Due to the lack of measured data, satellite images were used to calibrate the model by introducing the index of unmatched area (I_u) which is explained in the assessment indices section. In addition, various morphodynamic and numerical parameters were evaluated to find the superior model's parameters or calibrate the 2D depth-averaged model and evaluate the sensitivity of the model to these parameters. Superior model parameters are the best method or value in each parameter that gives the best results in this study. These parameters are cell size, roughness coefficient, transport functions, hiding functions, and bed roughness predictor. It should be noted that to evaluate the above-mentioned parameters, more than 80 numerical tests were done, generally. As these tests are time-consuming and the modeling of a braided river is complex, approximately 1.5 km of the river reach was considered in this step.

3.2.1 | Cell size and Manning roughness coefficient

Three different cell sizes of 2.5 × 2.5, 5 × 5, and 10 × 10 m^2 are evaluated in this study. Table 1 shows the results of these tests. According to this table, the results are better for the cell size of 5 × 5, 2.5 × 2.5, and 10 × 10 m^2, respectively. In addition, it should be noted that the cell size of 2.5 × 2.5 m^2 caused a very time-consuming simulation and the cell size of 10 × 10 m^2 could not consider the edges of the river properly. Therefore, the cell size of 5 × 5 m^2 is chosen as the best cell size in this study with the I_u of 52.79%.

According to the guidelines tables (Arcement & Schneider, 1989) and the Strickler roughness equation (Kim et al., 2010), and using the measured sediment distribution curve (Figure 2), the Manning roughness was extracted around 0.03. In addition, different values were

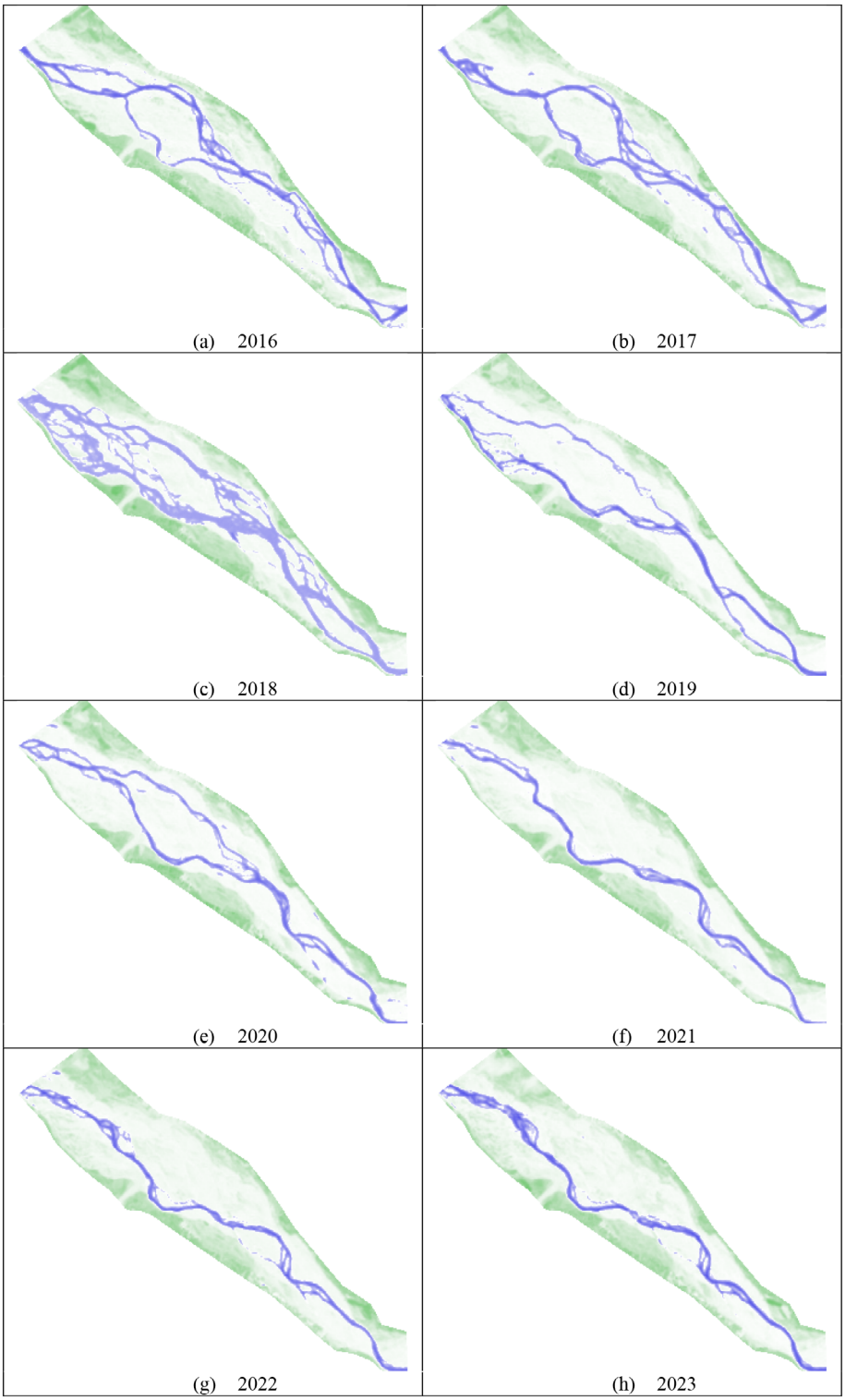

FIGURE 3 The Sentinel-2 L2A satellite images from 2016 (a) to 2023 (h) with NDWI for the focused reach of Devoll River. [Color figure can be viewed at wileyonlinelibrary.com]

tested to be sure about the calibration of this important parameter. Table 1 also shows the results of these tests for Manning roughness coefficient of 0.015, 0.03, 0.04, and 0.06. This table shows that the best models with the highest I_u are the Manning roughness coefficients of 0.03, 0.04, and 0.015 with I_u of 52.79, 51.01, and 50.92, respectively. Hence, the Manning roughness coefficient of 0.03 was chosen for this study.

3.2.2 | Transport function

One of the most effective parameters in morphodynamic modeling is the sediment transport function. In this study, 11 transport functions named Ackers and White, Engelund and Hansen, Laursen-Copeland, MPM, Toffaleti, MPM-Toffaleti, Yang, Wilcock and Crowe, Soulsby-Van Rijn, Van Rijn, and Wu et al. are evaluated and compared to each

other. Table 2 shows the unmatched water area (m^2) and I_u for these 11 transport functions. Best results extracted for the MPM, MPM-Toffaleti, Soulsby-Van Rijn, Wilcock and Crowe, Ackers and White, Engelund and Hansen, Yang, Toffaleti, Van Rijn, Wu et al., and Laursen-Copeland: with the I_u of 52.79%, 51.73%, 51.22%, 50.99%, 50.57%, 49.44%, 49.10%, 48.33%, 48.11%, 45.64%, and 44.17%, respectively. Therefore, Meyer-Peter and Müller's sediment function has the best agreement with observed water inundation and is chosen as the superior transport function in this study. It is noteworthy to observe that the modifications made in the Toffaleti transport function to derive the MPM-Toffaleti formula, specifically designed for gravel size, resulted in improved outcomes in this study, and the MPM-Toffaleti formula produced the second most precise results. Likewise, similar observations apply to the Van Rijn and Soulsby-Van Rijn models, in which Soulsby-Van Rijn has better results in modeling the braided river in this study compared to the Van Rijn transport function.

Figure 6 illustrates the comparison between simulated and observed water inundation areas in our study, using the MPM transport function for testing. In the figure, the blue area represents the observed region from the satellite image, the yellow area represents the depth-averaged simulation, and the red area represents the intersection of the simulated and observed water inundation areas (or common areas). It is important to note that to determine the exact simulated area, one should consider both the yellow and red areas. Similarly, for the observed area, both the blue and red areas should be taken into account.

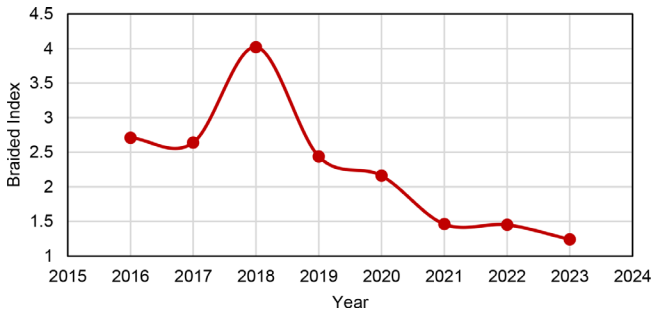

FIGURE 4 The braided index of Devoll River in 2016–2023. [Color figure can be viewed at wileyonlinelibrary.com]

The difference between the observed and simulated water inundation can originate from the resolution of the satellite image, classification of the model image to extract wet area, and resolution of the DTM file (i.e., input topography to the model), and so on, in addition to the numerical modeling. In addition to the parameters evaluated in this study, variation of roughness and slope along the river is effective. For example, the reach around zone A in Figure 6, has a high slope (0.039) compared to other reaches with an average value of 0.009, which shows the complexity of modeling this braided river.

Figure 7b represents the comparison of various transport functions in this study. Showing all these 11 transport functions in a graph makes the graph complex. Hence, just five transport functions such as MPM, Toffaleti, Soulsby-Van Rijn, Van Rijn, and Wu et al. have different topography results shown in Figure 7b. For example, one can see in this figure that the new topography caused by the Wu et al. transport function is different from Soulsby-Van Rijn, compared to the measured topography or DEM file. This is one reason that the water inundation area or unmatched area or I_u is different for each test.

Figure 7a shows the bed change for the test with the transport function of MPM. According to this figure, there is a deposition at the end of section A-A or at the beginning of the left branch, which is also observed in Figure 7b. This location with the deposition tendency was also observed in the field observation in 2022 (Figure 7c). Observing

FIGURE 5 Landslide in 2018 in the Devoll River. [Color figure can be viewed at wileyonlinelibrary.com]

Parameter	No.	Parameter value	Unmatched water area (m^2)	I_u (%)
Mesh size (m^2)	1	2.5 × 2.5	34411.26	51.61
	2	5 × 5	33570.35	52.79
	3	10 × 10	34132.19	52.00
Manning roughness coefficient	1	0.015	34896.65	50.92
	2	0.03	33570.35	52.79
	3	0.04	34835.16	51.01
	4	0.06	45831.24	35.55
	5	0.1	65083.73	8.47

TABLE 1 Sensitive analysis of the model to the mesh size and Manning roughness coefficient.

TABLE 2 Sensitive analysis of the model to the various transport functions.

No.	Transport functions	Unmatched water area (m^2)	I_u (%)
1	Meyer-Peter and Müller	33570.35	52.79
2	Van Rijn	36900.05	48.11
3	Toffaleti	36744.27	48.33
4	Laursen-Copeland	39699.04	44.17
5	Ackers and White	35145.61	50.57
6	MPM-Toffaleti	34322.03	51.73
7	Yang	36196.72	49.10
8	Wilcock and Crowe	34848.88	50.99
9	Soulsby-Van Rijn	34687.25	51.22
10	Wu et al.	38653.22	45.64
11	Engelund and Hansen	35949.24	49.44

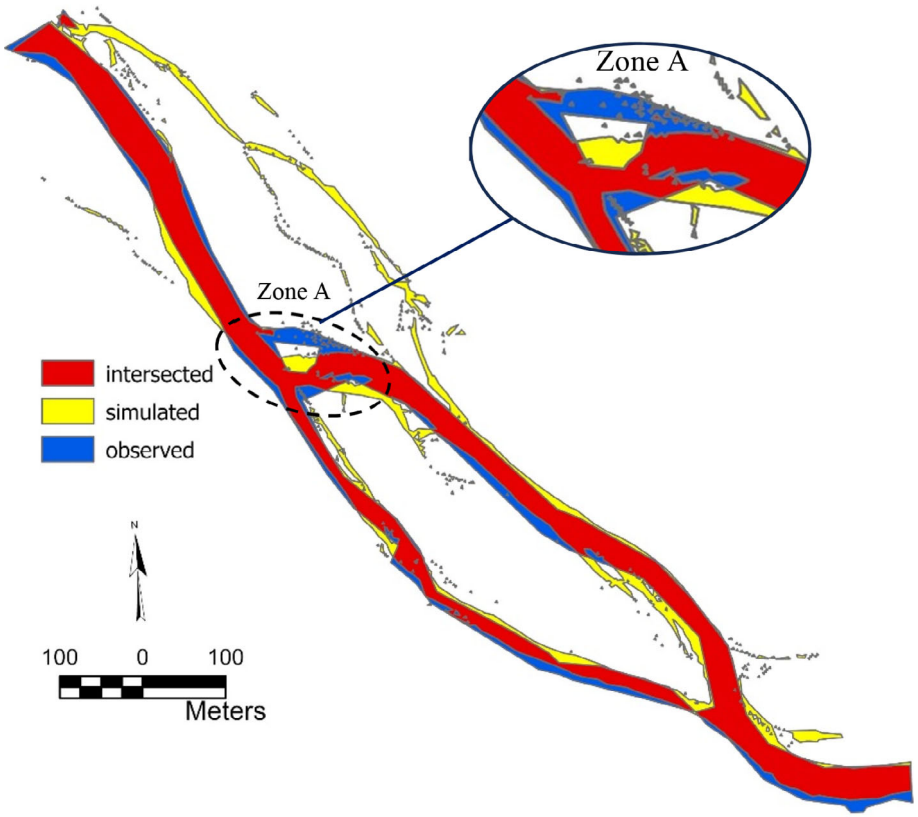

FIGURE 6 Comparison of the simulated and observed water inundation areas for the test with Meyer-Peter and Müller transport function. [Color figure can be viewed at wileyonlinelibrary.com]

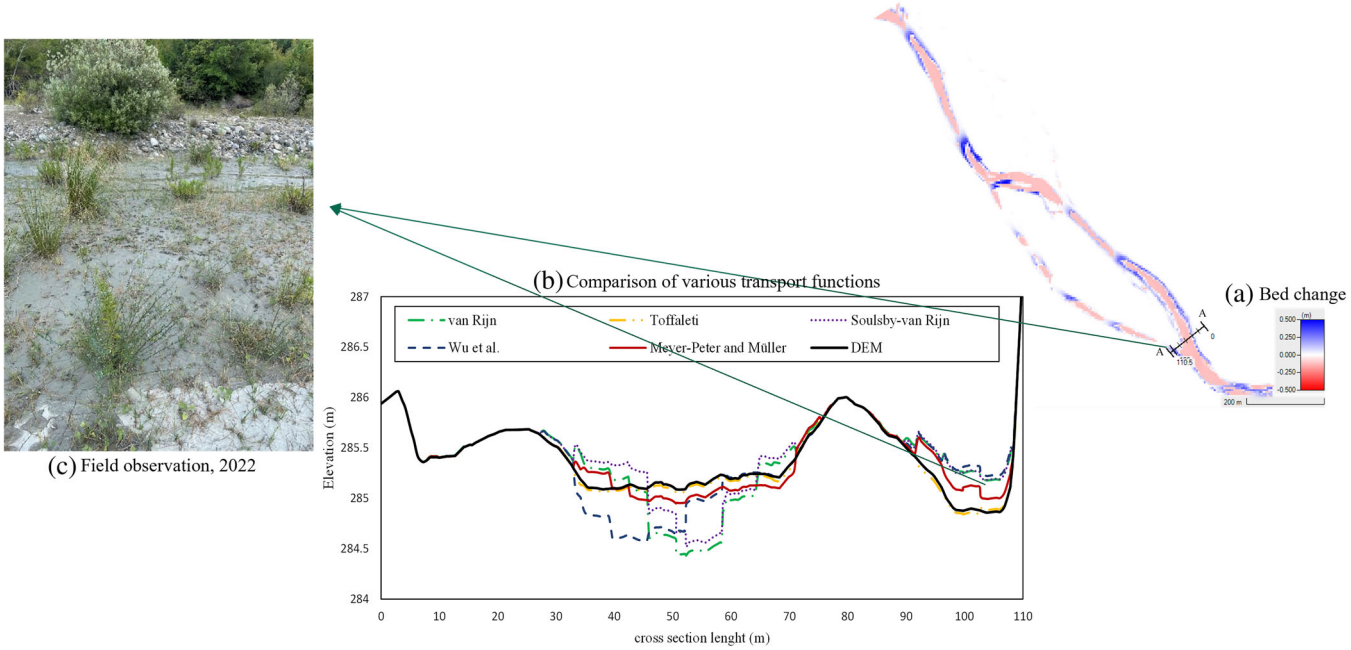

FIGURE 7 (a) Bed change of a test with Meyer-Peter and Müller transport function, (b) comparison of various transport functions on section A-A, and (c) field observation in 2022. [Color figure can be viewed at wileyonlinelibrary.com]

sediment deposition in the left branch in the field (2022), and the same happening in the current simulations gives one an indication that the results are in the right way.

3.2.3 | Hiding function

Another important parameter is the hiding function which represents the armor layer effect and it depends on the transport function and sediment distribution curve. The hiding functions used in this study are Ashida and Michiue (1971), Egiazaroff (1965), Hayashi et al. (1980), Parker et al. (1982), Wu et al. (2000), and a scenario without using the hiding function. Table 3 shows the results of the evaluation of these hiding functions. According to these results, the best results for this study are extracted for Ashida and Michiue (1971), Hayashi et al. (1980), not using the hiding function, Egiazaroff (1965), Parker et al. (1982), Wu et al. (2000) with the I_u values of 52.79, 51.70, 51.19, 50.23, 50.23, and 50.12, respectively. Despite the close proximity of the results from all functions, the study's findings suggest that the new probability approach (Wu et al., 2000) may not necessarily be the accurate hiding function.

Figure 8 shows the new topography caused by various mentioned hiding functions for section A-A (see Figure 7). It is obvious in this figure that Hayashi et al. (1980) caused more change to the morphodynamics of the river. In other words, Hayashi et al. (1980) are more effective in changing the topography of this complex braided river, and also more accurate with the highest I_u. It should be noted that the hiding functions of Ashida and Michiue (1971), Egiazaroff (1965), Parker et al. (1982), and Wu et al. (2000) caused less change in the topography and their results are similar to the initial topography (measured DEM).

3.2.4 | Bed roughness predictors

The bed roughness predictor parameter is an effective parameter that is rarely compared in the literature. As explained in Section 2, activation of this parameter gives the model of having a dynamic bed roughness to better consider the shape roughness and form roughness of the river. Table 4 shows the results of using various bed roughness predictors such as Brownlie, Limerinos, Van Rijn, and none or without using the bed roughness predictor. The best results were achieved using the Van Rijn, Limerinos, Brownlie, and none, with the I_u values of 58.67, 57.46, 52.97, and 52.79. Therefore, the superior bed roughness predictor scenario for this braided river case is Van Rijn. This result demonstrates that the assumption of considering the total roughness as the sum of the grain and dune roughness by Van Rijn (1984c) to predict bed roughness is more suitable compared to other methods for the braided river in this study.

3.3 | Effect of regulated discharge on the BI and morphodynamics of a braided river

As discussed before, the temporal variation of BI for the focused braided reach turns on a light that the regulated discharge caused a decrease in the BI of Devol River. To evaluate this assumption, a 2D morphodynamic model was calibrated for 1.5 km of the focused area and various effective sediment parameters were evaluated in Section 3.2. Then, in this section by extending the numerical modeling domain to 3 km akin to the used satellite images, two scenarios (a and b) were evaluated to investigate the above-mentioned assumption about the reduction of BI of Devoll braided river. In the first scenario

No.	Hiding functions	Unmatched water area (m^2)	I_u (%)
1	None (no correction)	34710.87	51.19
2	Hayashi et al. (1980)	33570.35	52.79
3	Wu et al. (2000)	35393.09	50.23
4	Parker et al. (1982)	35387.54	50.23
5	Egiazaroff (1965)	35467.08	50.12
6	Ashida and Michiue (1971)	34347.66	51.70

TABLE 3 Sensitive analysis of the model to the various hiding functions.

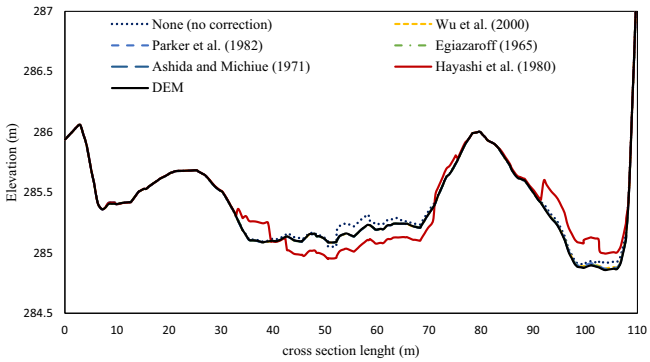

FIGURE 8 Effect of various hiding functions on the bed topography. [Color figure can be viewed at wileyonlinelibrary.com]

(a), the river reach is simulated from February 2016 to March 2023 using the regulated discharge hydrograph. In the second scenario (b), a natural, non-regulated discharge hydrograph based on hydrologic data for the same time period is utilized due to the absence of measured data for the entire period.

As approximately 3 years of 2D morphodynamic modeling of a complex braided river is time-consuming, some assumptions were considered to reduce the time cost of this modeling. First, various tests proved that discharges below 24 m^3/s are almost not effective on the sediment movement of this study. This type of assumption is also confirmed indirectly by Kasprak et al. (2019) used approximated a steady flow set of the peak discharge to reduce the time cost of the model. The next assumption is using the acceleration factor to decrease the time cost of the model. The factor is directly multiplied by the mass bed exchange rates at every time step (Hydrologic Engineering Center, 2021), and on the other hand, the time interval of the input hydrograph is divided by this factor manually. The acceleration factor reduced the 3-year simulation to the less than a month simulation (in addition to the first assumption which is removing discharge below 24 m^3/s). Finally, after considering the above-mentioned assumptions, the shortened hydrographs of both scenarios are shown in Figure 9. It should be noted according to the existing data, the flow with 1.5 m^3/s added to the released discharge from Moglice Dam due to the small lateral flows between the Moglice Dam and Kokel station (focused area of this study). In addition, other effective parameters used for these two modelings extracted from the calibration section are the cell size of 5×5 m^2, Manning roughness coefficient of 0.03, MPM transport function, Hayashi et al. (1980) hiding function, and Van Rijn bed roughness predictor. In the following

TABLE 4 Sensitive analysis of the model to the various bed roughness predictors.

No.	Predictor	Unmatched water area (m^2)	I_u (%)
1	None (no correction)	33570.35	52.79
2	Brownlie	33443.64	52.97
3	Limerinos	30251.43	57.46
4	Van Rijn	29389.07	58.67

subsections, the results of the 2D morphodynamic modeling of these two scenarios are discussed.

3.3.1 | BI variations

Two above-mentioned scenarios are modeled to investigate the assumption that released discharge from a hydropower dam with constant values around 30 or 70 m^3/s, instead of a natural hydrologic hydrograph with a gradually rising phase, peak, and then gradually receding phase is one of the reasons for decreasing BI or straightening of Devoll River. The velocity patterns of the end of the simulation of these two scenarios are shown in Figure 10a,b. According to this figure, one can see the active channels in this braided reach which are more in scenario B in comparison with scenario A.

Results of computing the BI of these two scenarios show that the BI for scenario A is 1.71 and for scenario B is 2.62. These results have an agreement with the temporal variation of BI by satellite images with the BI of 1.24 for March of 2023 (Section 3.1). Although there are some uncertainties in the modeling to be checked in the future, these results showed that one of the reasons that caused the braided river to be straight is a regulated discharge hydrograph instead of a natural hydrological discharge hydrograph.

3.3.2 | Bed change and shear stress variations

The bed change map of these two scenarios is shown in Figure 10c,d. According to this figure, there is more deposition in scenario A which used the regulated hydrograph, compared to scenario B which used a non-regulated type of hydrologic data. Hence, this can be one reason for decreasing the BI, because more deposition can be caused by blocking more reaches. For example, in Figure 10c, zone 4 shows that the deposition blocks the lateral branches in this zone, as well as zone 2. In the top part of zone 1, there is a bar formed in comparison with

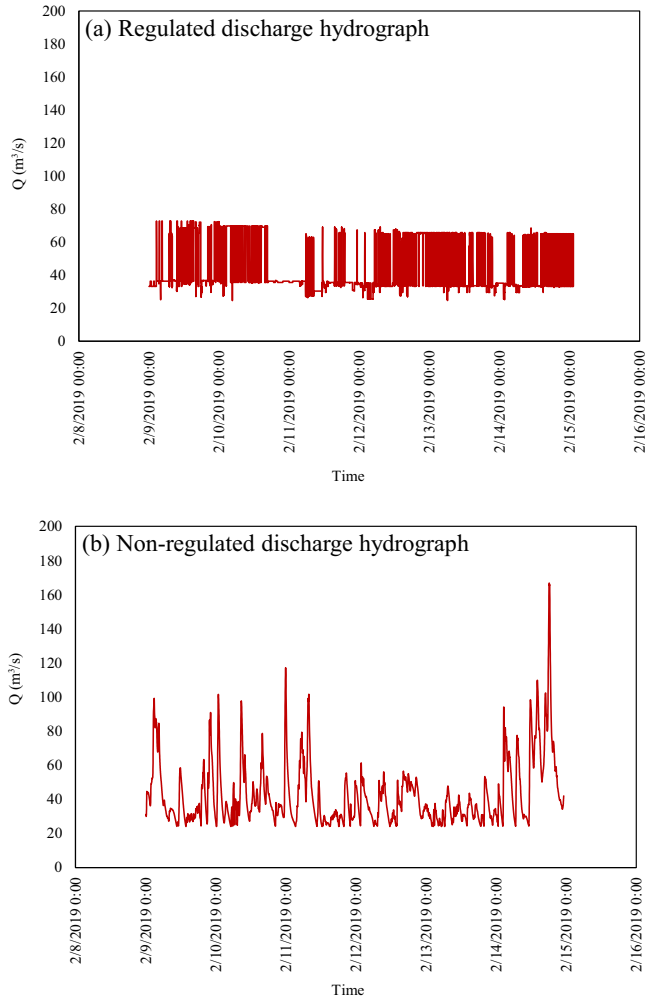

FIGURE 9 Input discharge hydrographs of two scenarios. [Color figure can be viewed at wileyonlinelibrary.com]

scenario B, which may cause some changes in the future in this zone. In addition, at the bottom of zone 1, a new branch is activated which is not visible in scenario B. In addition to the uncertainties that exist in this study, and also due to the fact that braiding is a completely random phenomenon and all details occurred in the river reach can be effective, this small reach at the bottom of zone 1 can be an occurred due to the starting point of simulation as it is started at the beginning of a bend, or it might happen in the future and the curve shape changed after some years which will be evaluated in the future studies.

Figure 10e,f shows the bed shear stress of these two scenarios. According to this figure, for scenario B more active reaches were observed in the bed shear stress map with yellow color, compared to scenario A. In addition, locations with high bed shear stress are also observed in this figure. Higher shear stress values occurred mainly in the main channel.

3.3.3 | Total load transport rate and suspended load concentration

Zone 3 of Figure 10c was chosen to represent the temporal variation of the total load transport rate and suspended load concentration due to the fact that this zone is in the main channel and there are no other branches in this cross section. Figure 11a,b shows the results of the total load transport rate (kg/m/s) for both scenarios. This figure shows that the maximum values of total bed load rate (kg/s/m) are 35.93 and 16.32 for scenarios A and B, respectively. Therefore, one can conclude that using the regulated discharge hydrograph from the upstream dam can cause more total load transport rate compared to the natural hydrologic discharge hydrograph. This can be the reason for decreasing the BI of the river in scenario A, compared to scenario B.

Figure 11c,d shows the results of the suspended load concentration (mg/l) for both scenarios. This figure shows that the maximum values of suspended load concentration (mg/l) are 652.48 and 152.39 for scenarios A and B, respectively. Therefore, similar to the results of Figure 11a,b, Figure 11c,d shows that using the scenario with the regulated discharge hydrograph can cause more suspended load concentration compared to the scenario with a non-regulated discharge hydrograph, in this study. This can also be the reason for decreasing the BI of the river in scenario A, compared to scenario B.

It should be noted that the effect of bedload and suspended load coming from upstream of the focused area is not considered in this study. Hence, these results can be attributed to the shapes of the regulated and non-regulated discharge hydrograph scenarios, as elucidated in the previous sections.

These interesting results from the total load transport rate and suspended load concentration underscore the significant impact exerted by the released regulated discharge from the upstream hydropower dam. Therefore, using discharge hydrograph from hydrologic modeling without considering real scenarios like regulated discharge should be considered more cautiously.

4 | CONCLUSION

The study of braided rivers is essential for understanding the complex interactions between hydrodynamics, sediment transport, and ecosystem dynamics. This study aimed to address existing gaps in evaluating the morphodynamics and complexity of braided rivers by analyzing the temporal variation of the BI through satellite images and 2D morphodynamic modeling.

In this context, our study has made several contributions to the existing body of knowledge:

1. 2D morphodynamic modeling: Through an extensive series of numerical tests, various parameters, including three cell sizes, five Manning roughness coefficients, 11 transport functions, five hiding functions, and three bed roughness predictors, were evaluated. The results indicated that specific parameter values, including a cell size of $5 \times 5\ m^2$, a Manning roughness coefficient of 0.03, the MPM sediment transport function, Hayashi et al. (1980) hiding function, and Van Rijn bed roughness predictor produced the best agreement with observed water inundation.
2. Temporal variation of the BI: In general, the analysis of satellite images revealed a gradual decrease in the braided intensity of the

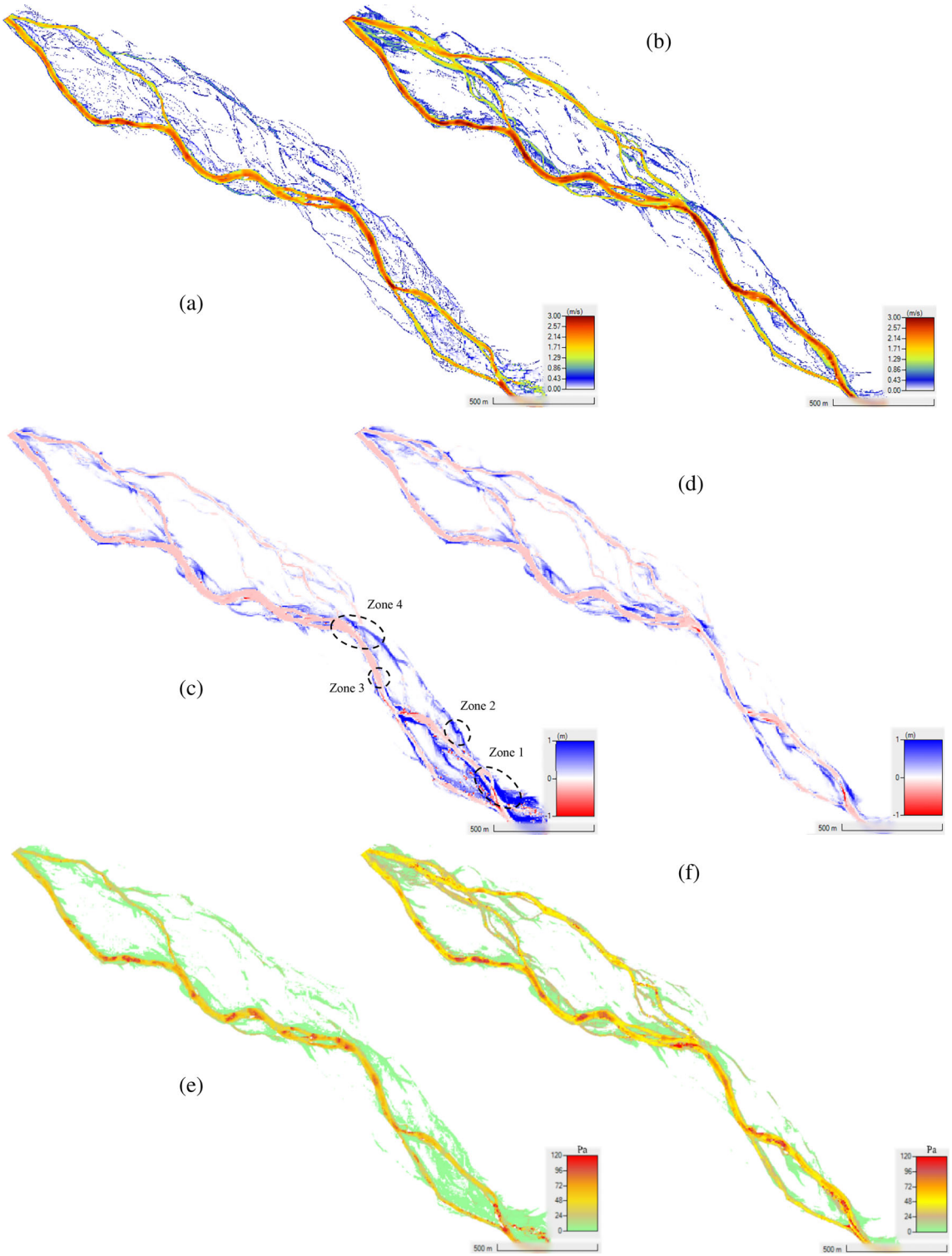

FIGURE 10 Velocity, bed changes, and bed shear stress patterns of scenario with the regulated discharge hydrograph (a, c, and d, respectively), and for the scenario with the non-regulated discharge hydrograph (b, d, and f, respectively). [Color figure can be viewed at wileyonlinelibrary.com]

Devoll River from 2016 to 2023, declining from 2.17 to 1.24, respectively. However, this trend was punctuated by an anomalous increase in 2018, which can be attributed to the influence of external factors, such as a landslide event in 2018.

3. Regulated discharge-hydrograph impact: The dam's regulation of discharge is a key factor in altering the river's behavior, leading to a reduction in braiding intensity. This effect was particularly pronounced following the dam's impoundment, indicating the role of

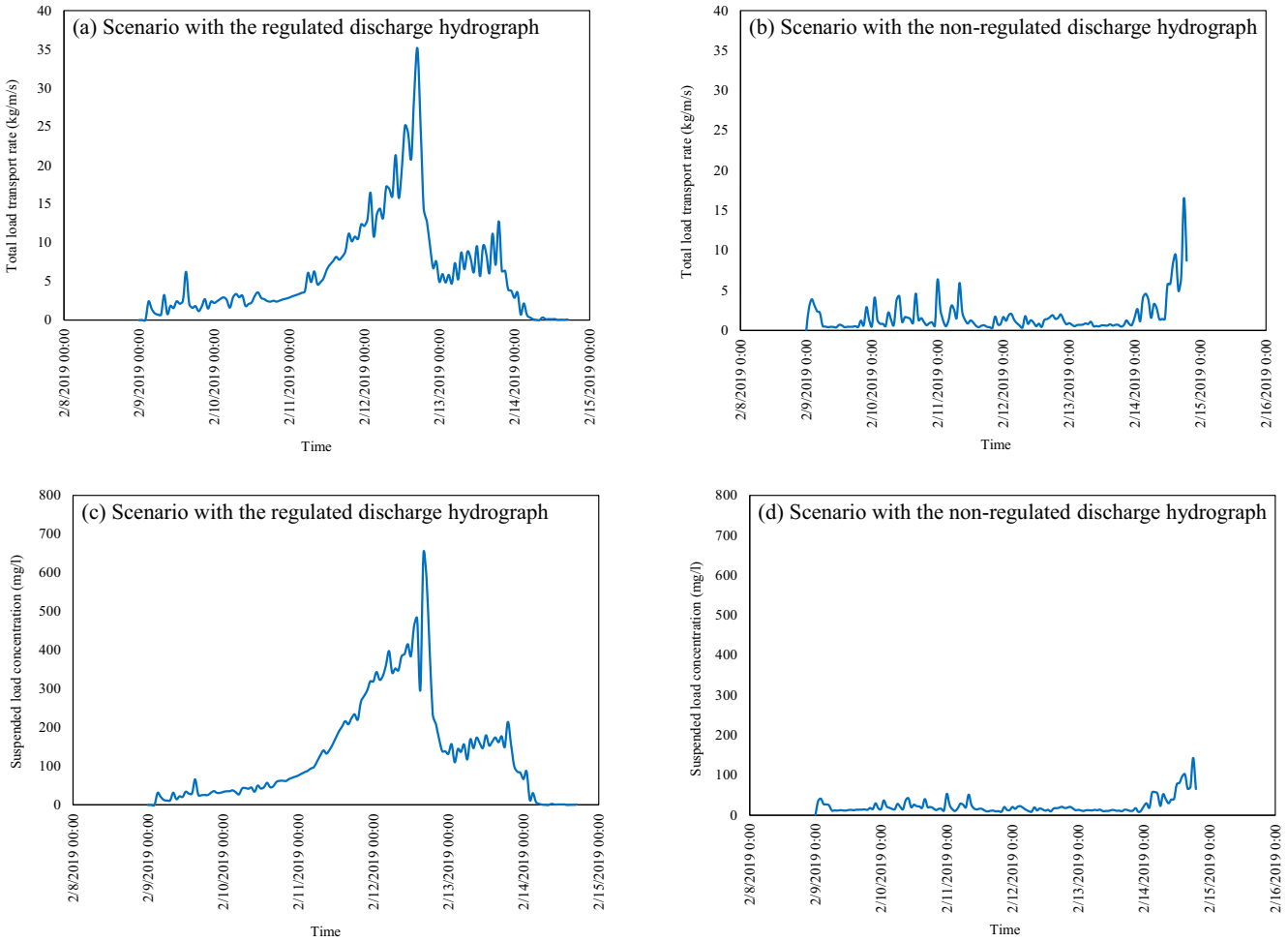

FIGURE 11 Total load transport rate and suspended load concentration for both scenarios A and B. [Color figure can be viewed at wileyonlinelibrary.com]

hydropower operations in river channel adjustments.

Comparing two scenarios, one using the regulated discharge hydrograph and the other using natural hydrologic data or non-regulated discharge hydrograph, indicated that the former resulted in lower braiding and more deposition.

4. Total load transport and suspended load concentration: The modeling results revealed that the regulated discharge hydrograph scenario led to higher total load transport rates (35.93 kg/s/m) and suspended load concentrations (652.48 mg/L) compared to the natural hydrologic data (16.32 kg/s/m and 152.39 mg/L). This suggests that the regulated discharge released by hydropower dam altered flow regime has downstream effects on sediment transport, which in turn influences the river's morphology.

In summary, this study underscores the intricate interplay between natural processes and human interventions in shaping the morphodynamics of braided rivers. The findings emphasize the importance of considering not only natural hydrological data but also the specific impacts of dam operations in river management and restoration efforts. Such insights are vital for sustainable river basin management and ecological preservation, ensuring the long-term health and resilience of these unique and dynamic river systems.

ACKNOWLEDGMENTS

This study was carried out within the framework of the DIRT-X project, which is part of AXIS, an ERA-NET initiated by JPI Climate, and funded by FFG Austria, BMBF Germany, FORMAS Sweden, NWO NL, and RCN Norway with co-funding from the European Union (Grant No. 776608). The authors express their gratitude to Killian Mouris, Mahmoud Saber Kenawi, Slaven Conevski, Ayda Mirzaahmadi, Agim Lazareni, and Florenc Kasmi, as well as other supportive friends and colleagues who provided valuable assistance throughout this study.

CONFLICT OF INTEREST STATEMENT

The authors declare no conflicts of interest related to the research, authorship, or publication of this manuscript.

DATA AVAILABILITY STATEMENT

The data supporting the findings of this study are available upon request from the corresponding author.

ORCID

Behnam Balouchi https://orcid.org/0000-0001-8750-0275

REFERENCES

Ackers, P., & White, W. R. (1973). Sediment transport: New approach and analysis. *Proceedings. ASCE, Journal of the Hydraulic Division*, *99*(HY11), 2041–2060.

Antoniazza, G., Bakker, M., & Lane, S. N. (2019). Revisiting the morphological method in two dimensions to quantify bed-material transport in braided rivers. *Earth Surface Processes and Landforms*, *44*, 2251–2267. https://doi.org/10.1002/esp.4633

Hayashi, T. S., Ozaki, S., & Ichibashi, T. (1980). Study on bed load transport of sediment mixture. In *Proc. 24th Japanese Conf. on Hydraulics*. Japan Society of Civil Engineers.

Arcement, G. J., Jr., & Schneider, V. R. (1989). Guide for selection Manning's roughness coefficients for natural channels and flood plains. Water-resource paper 2339, U.S. Geological Survey.

Ashida, K., & Michiue, M. (1971). An investigation of river bed degradation downstream of a dam. *Proc. 14th congress of IAHR*, *3*, 247–256.

Ashmore, P. E. (1982). Laboratory modelling of gravel braided stream morphology. *Earth Surface Processes and Landforms*, *7*(3), 201–225. doi:10.1002/esp.3290070301

Ashworth, P. J., Best, J. L., & Jones, M. A. (1994). Relationship between sediment supply and avulsion frequency in braided rivers. *Geology*, *32*(1), 21–24. doi:10.1130/g19919.1

Balouchi, B., Rüther, N., & Valerie Anne Schwarzwälder, K. (2023). Temporal analysis of the Braided River index by satellite images. In *proceedings of the 40th IAHR world congress, 21–25 August 2023*. International Association for Hydro-Environment Engineering and Research (IAHR).

Balouchi, B., Rüther, N., Mirzaahmadi, A., & Valerie Anne Schwarzwälder, K. (2022). 2D depth-averaged numerical modeling of a braided river morphodynamics. In *7th IAHR Europe congress innovative water Management in a Changing Climate, September 2022*. International Association for Hydro-Environment Engineering and Research (IAHR).

Bertoldi, W., Zanoni, L., & Tubino, M. (2010). Assessment of morphological changes induced by flow and flood pulses in a gravel bed braided river: The Tagliamento River (Italy). *Geomorphology*, *114*, 348–360. https://doi.org/10.1016/j.geomorph.2009.07.017

Brownlie, W. R. (1983). Flow depth in sand-bed channels. *Journal of Hydraulic Engineering, ASCE*, *109*(7), 959–990.

Copeland, R. R., & Thomas, W. A. (1989). Corte Madera Creek sedimentation study. In *Numerical model investigation, TR-HL-89-6. US Army waterways Experiment Station*. US Army Corps of Engineer (USACE).

Day, T. J. (1980). A study of the transport of graded sediments. Report N. IT 190, HR Wallingford, U.K.

Deltares. (2011). *Delft3D-FLOW, simulation of multi-dimensional hydrodynamic flows and transport phenomena*. Including Sediments, User Manual: Hydro-Morphodynamics.

Dubey, A. K., Chembolu, V., & Dutta, S. (2020). Utilization of satellite altimetry retrieved river roughness properties in hydraulic flow modelling of braided river system. *International Journal of River Basin Management*, *20*, 411–424. https://doi.org/10.1080/15715124.2020.1830785

Egiazaroff, I. V. (1965). Calculation of nonuniform sediment concentration. *Journal of Hydraulic Division, ASCE*, *91*(HY4), 225–247.

Egozi, R., & Ashmore, P. E. (2009). Experimental analysis of braided channel pattern response to increased discharge. *Journal of Geophysical Research: Earth Surface*, *114*, F02012. https://doi.org/10.1029/2008jf001099

Engelund, F., & Hansen, E. (1967). *A monograph on sediment transport in alluvial streams* (p. 65). Teknisk Forlag.

Faeh, R., Mueller, R., Rousselot, P., Vetsch, D., Volz, C., Vonwiller, L., Veprek, R., & Farshi, D. (2011). System manuals of BASEMENT, version 2.1. ETH Zürich: Laboratory of hydraulics, glaciology, and hydrology three-dimensional versus two-dimensional approaches. *Geomorphology*, *29*(1–2), 1–20.

Hafen, K., & Kasprak, A. (2019). The MoRPHED morphodynamic model, source code. https://github.com/morphed/MoRPHED

Hervouet, J. M., & Ata, R. (2017). User manual of open-source software TELEMAC-2D. EDF-R&D. https://www.opentelemac.org/. (Version: V7P2)

Hydrologic Engineering Center. (2021). *HEC-RAS 2D modeling User's manual*. U.S. Army Corps of Engineers.

International Hydropower Association. (2022). Sediment management case study: Albania Devoll. Hydropower.org, https://www.hydropower.org/sediment-management-case-studies/albania-devoll

Kasprak, A., Ashmore, P. E., Hensleigh, J., Peirce, S., & Wheaton, J. M. (2015). The relationship between particle travel distance and channel morphology: Results from physical models of braided rivers. *Journal of Geophysical Research: Earth Surface*, *120*(1), 55–74. https://doi.org/10.1002/2014jf003310

Kasprak, J., Brasington, J., Hafen, K., Williams, R. D., & Wheaton, J. M. (2019). Modelling braided river morphodynamics using a particle travel length framework. *Earth Surface Dynamics*, *7*, 247–274. https://doi.org/10.5194/esurf-7-247-2019

Kim, J. S., Lee, C. J., Kim, W., & Kim, Y. J. (2010). Roughness coefficient and its uncertainty in gravel-bed river. *Water Science and Engineering*, *3*, 217–232.

Kuo, C.-W., Chen, C.-F., Chen, S.-C., Yang, T.-C., & Chen, C.-W. (2017). Channel planform dynamics monitoring and channel stability assessment in two sediment-rich rivers in Taiwan. *Water*, *9*, 84.

Laursen, E. M. (1958). The total sediment load of streams. *Journal of Hydraulic Division, ASCE*, *84*(1), 1–36.

Limerinos, J. T. (1970). Determination of the manning coefficient for measured bed roughness in natural channels. In *Water supply paper 1898-B, U.S. Geological Survey*. U.S. Govt. Print. Off.

Lotsari, E. S., Calle, M., Benito, G., Kukko, A., Kaartinen, H., Hyyppä, J., Hyyppä, H., & Alho, P. (2018). Topographical change caused by moderate and small floods in a gravel bed ephemeral river—A depth-averaged morphodynamic simulation approach. *Earth Surface Dynamics*, *6*, 163–185. https://doi.org/10.5194/esurf-6-163-2018

Meyer-Peter, E., & Müller, R. (1948). Formulas for bed-load transport. In *Proceedings of the 2nd congress IAHR*. IAHR.

Mouris, K., Schwindt, S., Haun, S., Morales Oreamuno, M. F., & Wieprecht, S. (2022). Introducing seasonal snow memory into the RUSLE. *Journal of Soils and Sediments*, *22*, 1609–1628. https://doi.org/10.1007/s11368-022-03192-1

Norconsult. (2011). Devoll hydropower project. ESIA Final Report.

Okazaki, S. (2001). A note on the calculation of Egiazaroff for nonuniform sediment concentrations. *Science Reports of Tohoku University*, *51*, 35–44.

Olsen, N. R. B. (2021). 3D numerical modelling of braided channel formation. Journal of. *Geomorphology*, *375*, 107528.

Paixão, M., & Kobiyama, M. (2020). Sediment transport for nonuniform sediment mixtures: The Egiazaroff equation and its application in a canyon river in Brazil. *Ciência e Natura*, *42*(e40), 10. https://doi.org/10.5902/2179460X39297

Parker, G., Klingeman, P. C., & McLean, D. G. (1982). Bed load and size distribution in paved gravel-bed streams. *Journal of the Hydraulics Division, ASCE*, *108*(4), 544–571.

Pesci, M. H., Mouris, K., Haun, S., & Förster, K. (2023). Assessment of uncertainties in a complex modeling chain for predicting reservoir sedimentation under changing climate. *Modeling Earth Systems and Environment.*, *9*, 3777–3793. https://doi.org/10.1007/s40808-023-01705-6

Prasujya, G., & Nayan, S. (2021). Spatio-temporal study of morpho-dynamics of the Brahmaputra River along its Majuli Island reach. *Environmental Challenges*, *5*, 100217. https://doi.org/10.1016/j.envc.2021.100217

Proffitt, G. T., & Sutherland, A. J. (1983). Transport of nonuniform sediment. *Journal of Hydraulic Research, IAHR*, *21*(1), 33–43.

Schendel, A., Goseberg, N., & Schlurmann, T. (2015). Erosion stability of wide-graded quarry-stone material under unidirectional current.

Journal of Waterway, Port, Coastal and Ocean Engineering, *142*(3), 04015023. https://doi.org/10.1061/(ASCE)WW.1943-5460.0000321

Schuurman, F., Marra, W., & Kleinhans, M. (2013). Physics-based modeling of large braided sand-bed rivers: Bar pattern formation, dynamics, and sensitivity. *Journal of Geophysical Research: Earth Surface*, *118*(5), 2509–2527. https://doi.org/10.1002/2013JF002896

Shampa, M. M. A. (2019). Interaction between the braided bar and adjacent channel during flood: A case study of a sand-bed braided river, Brahmaputra–Jamuna. *Sustainable Water Resources Management*, *5*, 947–960. https://doi.org/10.1007/s40899-018-0269-x

Soulsby, R. L. (1997). *Dynamics of marine sands*. Thomas Telford Publications.

Sun, J., Lin, B., & Yang, H. (2015). Development and application of a braided river model with non-uniform sediment transport. *Advances in Water Resources*, *81*, 62–74. https://doi.org/10.1016/j.advwatres.2014.12.012

Toffaleti, F. B. (1968). A procedure for computation of total river sand discharge and detailed distribution, bed to surface. Technical Report No. 5, Committee on Channel Stabilization, U.S. Army Corps of Engineers, November.

Van Rijn, L. C. (1984a). Sediment transport, part I: Bed load transport. *Journal of Hydraulic Engineering, ASCE*, *110*(10), 1431–1456.

Van Rijn, L. C. (1984b). Sediment transport, part II: Suspended load transport. *Journal of Hydraulic Engineering, ASCE*, *110*(11), 1613–1641.

Van Rijn, L. C. (1984c). Sediment transport: Part III: Bed form and alluvial roughness. *Journal of Hydraulic Engineering*, *110*(12), 1733–1754.

Van Rijn, L. C. (1993). *Principles of sediment transport in river, estuaries, coastal seas, and oceans*. International Institute for Infrastructural, Hydraulic, and Environmental Engineering.

Vanoni, V. A. (1975). Sedimentation engineering practice. *American Society of Civil Engineers, Manuals and Reports on Engineering Practice*, *54*, 745.

Wilcock, P. R., & Crowe, J. C. (2003). Surface-based transport model for mixed-size sediment. *Journal of Hydraulic Engineering*, *129*(2), 120–128.

Williams, D. T., & Julien, P. Y. (1989). Applicability index for sand transport equations. *Journal of Hydraulic Engineering*, *115*(11), 1578–1581.

Williams, R. D., Brasington, J., & Hicks, D. M. (2016). Numerical modelling of Braided River Morphodynamics: Review and future challenges. *Geography Compass*, *10*(3), 102–127. https://doi.org/10.1111/gec3.12260

Williams, R. D., Measures, R., Hicks, D. M., & Brasington, J. (2016). Assessment of a numerical model to reproduce event-scale erosion and deposition distributions in a braided river. *Water Resources Research*, *52*, 6621–6642. https://doi.org/10.1002/2015WR018491

Wu, W. (2007). *Computational river dynamics*. Taylor & Francis.

Wu, W., Wang, S. S. Y., & Jia, Y. (2000). Non-uniform sediment transport in alluvial rivers. *Journal of Hydraulic Research, IAHR*, *38*(6), 427–434.

Yang, C. T. (1973). Incipient motion and sediment transport. *Journal of the Hydraulics Division*, *99*(HY10), 1006–1007.

Yang, C. T. (1979). Unit stream power equations for total load. *Journal of Hydrology*, *40*, 123–128.

Yang, C. T. (1984). Unit stream power equation for gravel. *Journal of Hydraulic Division, ASCE*, *110*(12), 1783–1797.

Yang, H. (2020). Numerical investigation of avulsions in gravel-bed braided rivers. *Hydrological Processes*, *34*, 3702–3717. https://doi.org/10.1002/hyp.13837

Yassine, R., Cassan, L., Roux, H., Frysou, O., & Pérès, F. (2023). Numerical modelling of the evolution of a river reach with complex morphology to help define future sustainable restoration decisions. *Earth Surface Dynamics*, *11*, 1199–1221. https://doi.org/10.5194/esurf-11-1199-2023

You, Y., Li, Z., Gao, P., & Hu, T. (2022). Impacts of dams and land-use changes on hydromorphology of braided channels in the Lhasa River of the Qinghai-Tibet plateau, China. *International Journal of Sediment Research*, *37*, 214–228.

How to cite this article: Balouchi, B., Rüther, N., & Schwarzwälder, K. (2024). Temporal variation of braided intensity and morphodynamic changes in a regulated braided river using 2D modeling and satellite images. *River Research and Applications*, 1–17. https://doi.org/10.1002/rra.4268